ELSEVIER

Nuclear Instruments and Methods in Physics Research B 148 (1999) 957–963

NIM B
Beam Interactions with Materials & Atoms

Microstructure of sulfide nanocrystals formed by ion-implantation

A. Meldrum [a,*], C.W. White [a], L.A. Boatner [a], I.M. Anderson [a], R.A. Zuhr [a], E. Sonder [a], J.D. Budai [a], D.O. Henderson [b]

[a] *Oak Ridge National Laboratory, Solid State Division, MS-6057, Oak Ridge, TN USA*
[b] *Fisk University, Department of Physics, Nashville, TN, USA*

Abstract

Ion implantation is a versatile tool for the formation of compound semiconductor nanocrystal precipitates in a host medium with the ultimate goal of producing a uniform size distribution of quantum dots for use in optical devices. Ion implantation was used to form ZnS, CdS, and PbS nanocrystals in both glass and crystalline hosts, and the precipitate microstructures and size distributions were investigated by TEM techniques. The size distributions were found to be significantly different for the three compounds, and several unusual microstructures were observed. © 1999 Elsevier Science B.V. All rights reserved.

PACS: 61.46; 61.16.B
Keywords: Nanocrystals; Sulfides; Ion implantation; ZnS; CdS; PbS

1. Introduction

Interest in the properties of sulfide nanocrystals stems from their potential use in non-linear optical devices. The opto-electronic properties of nanocrystalline semiconductor materials are significantly different as compared to their bulk analogues. Thus far, the potential device applications of these materials have been limited by the inability to create a large volume-filling fraction of nanocrystals in an appropriate optical host. In addition, a narrow particle size distribution is often desirable for non-linear device applications. Ion implantation is currently being investigated as a means of synthesizing embedded single-element and compound nanocrystals, and the use of this technique to form nanocrystals of CdS, ZnS, and PbS in both amorphous and crystalline hosts has been previously reported [1–3]. The size distributions of nanocrystals formed by this approach, however, are such that no fine structure originating from quantized transitions has been observed in the optical absorption or photoluminescence spectra. The goal of the present study is to use TEM techniques to systematically investigate the main factors affecting the size distribution and microstructures of sulfide nanocrystal precipitates produced by ion-implantation-synthesis techniques

* Corresponding author. Tel.: +1 423 241 5116; fax: +1 423 576 8135; e-mail: al-m@worldnet.att.net

0168-583X/98/$ – see front matter © 1999 Elsevier Science B.V. All rights reserved.
PII: S0168-583X(98)00727-7

Table 1
Implant and annealing conidtions for the specimens shown in Figs. 1–5. The dose is given in units of ion/cm^2, except for the multi-energy samples – for which it is given as a concentration of impurity ions in ions/cm^3 (italics), obtained from the RBS results. The average particle diameter and standard deviation (a measure of the size distribution) are given in the final two columns. These values were not obtained for Al_2O_3–PbS and Al_2O_3–Zns because many of the nanocrystals coalesced to form a semi-continuous layer

Specimen	Implant conditions				Annealing conditions			Measurements	
	Cation energy (keV)	Anion energy (keV)	Dose	Temperature (K)	Atmosphere	Time (min)	Temperature (K)	Average size (nm)	Standard deviation
SiO_2–ZnS-1	Multi		0.5×10^{21}	300	ArH_2	60	1000	2.4	0.4
SiO_2–ZnS-2	Multi		6.5×10^{21}	300	ArH_2	60	1000	7.5	5.3
SiO_2–ZnS-3	320	180	1.0×10^{17}	300	ArH_2	6	1000	6.5	3.9
SiO_2–ZnS-4	Multi		5.0×10^{21}	300	ArH_2	60	1000	7.8	6.1
SiO_2–CdS-1	Multi		0.8×10^{21}	300	ArH_2	60	1000	4.9	1.3
SiO_2–CdS-2	Multi		0.2×10^{21}	300	ArH_2	60	1000	6.5	2.2
SiO_2–CdS-3	Multi		5.3×10^{21}	300	ArH_2	60	1000	9.8	3.6
SiO_2–PbS-1	320	82	2.5×10^{16}	300	ArH_2	60	1000	6.8	3.4
SiO_2–PbS-2	320	82	7.5×10^{16}	300	ArH_2	60	1000	8.5	9.5
Al_2O_3–ZnS	280	150	6.0×10^{16}	700	ArH_2	60	1000	Not obtained	
Al_2O_3–CdS	450	164	4.3×10^{16}	900	ArH_2	60	1000	17.7	12.4
Al_2O_3–PbS	850	180	5.0×10^{16}	850	ArH_2	60	1000	Not obtained	

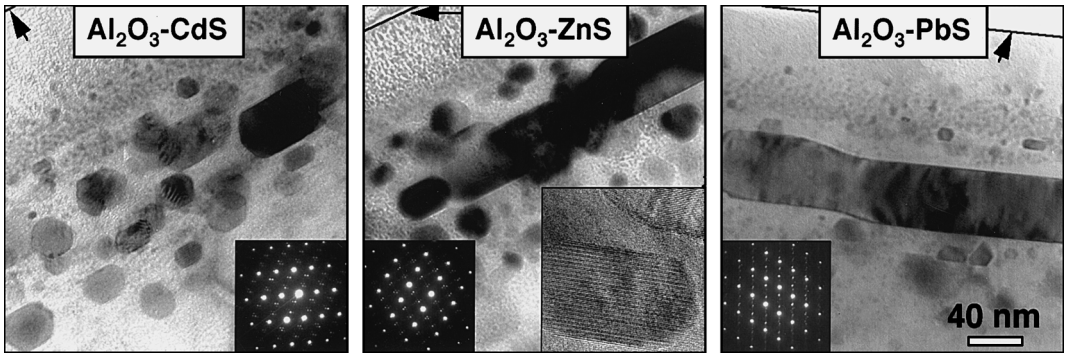

Fig. 1. Sulfide nanocrystals in α-Al_2O_3. The arrows point to the sample surface.

and to find avenues by which narrow precipitate size distributions and simple microstructures may be realized.

2. Experimental

Ion implantation of the component elements followed by thermal annealing was used to form ZnS, CdS, and PbS nanocrystal precipitates in high-purity fused silica and (0 0 1)-oriented α-Al_2O_3 hosts. Ion energies were selected using the TRIM-96 code so as to give overlapping concentration profiles, and equal doses were used to give the proper stoichiometry. In some cases, multi-energy implants were carried out in order to obtain a spatially uniform concentration profile of each constituent. A reference list of the implant and annealing conditions used for the specimens investigated here is given in Table 1. Rutherford Backscattering Spectrometry (RBS) using 2.3 MeV He^+ ions and a detector angle of 160° was used to measure the concentration profiles of the as-implanted and annealed samples.

Cross-sectional specimens were prepared for TEM analysis by gluing the implanted face to a Si wafer and hand-polishing to a thickness of ~1 μm, as estimated by the color of the Si in transmitted light [4]. The specimens were then attached to a copper grid and ion milled for 15–45 min at liquid nitrogen temperature using 4 keV Ar^+ ions and a beam current of 1 mA. This technique generally provides large thin areas containing the implanted

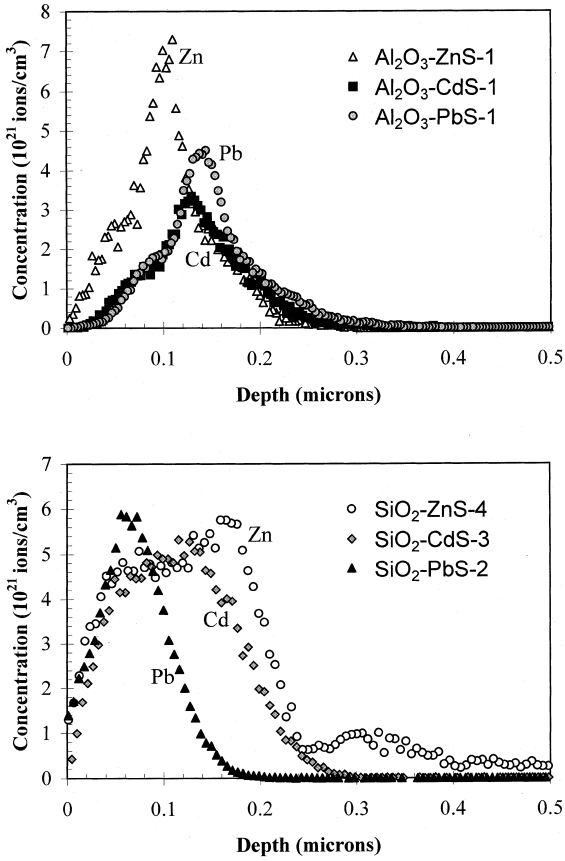

Fig. 2. Representative cation depth-concentration profiles after annealing, as obtained by RBS. Sample descriptions are given in Table 1.

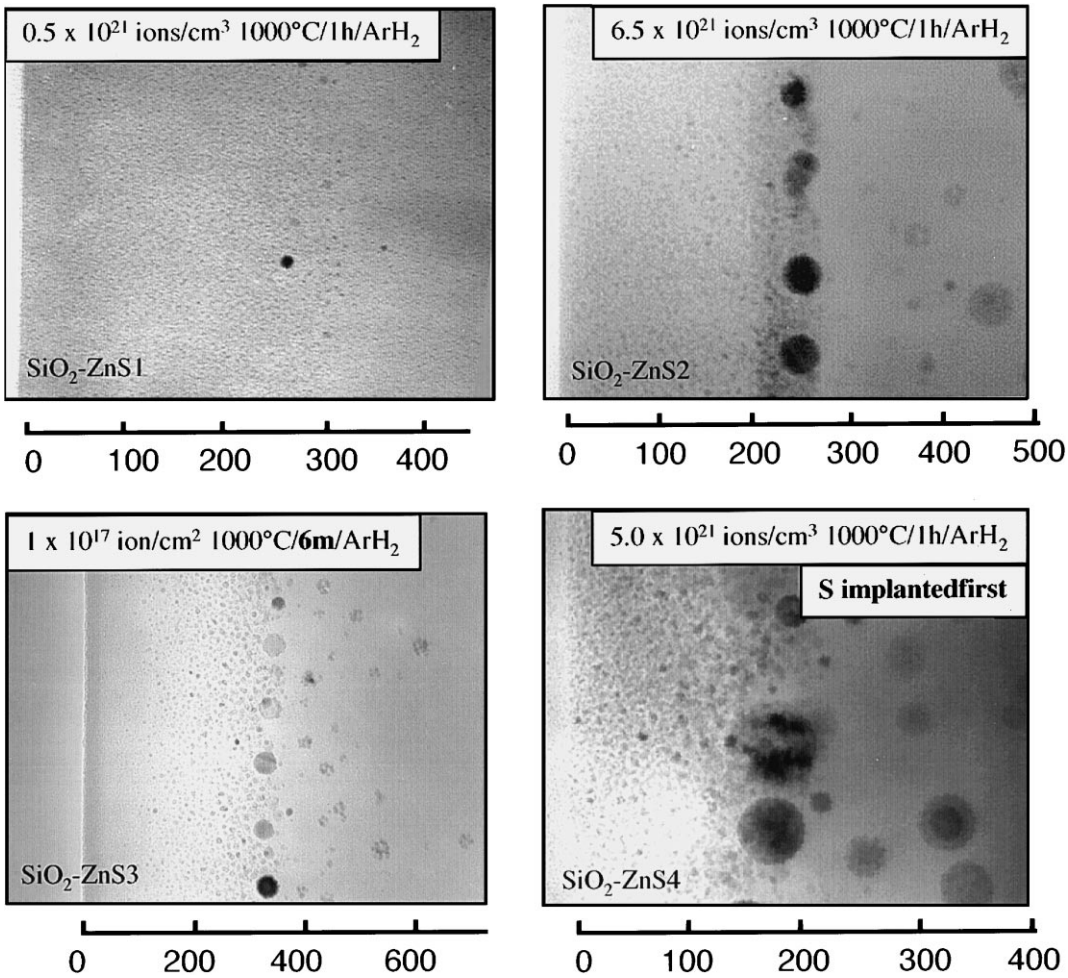

Fig. 3. Cross-sectional TEM images of ZnS nanoparticles in fused silica. The depth scale is in nanometers. Sample numbers are given in the lower left corner of each image, and the implant dose (or concentration in the case of the multi-energy implants) and annealing conditions (temperature/time/atmosphere) are given at the top.

nanocrystals. Standard TEM analysis was performed using a Philips EM400 electron microscope operated at 100 keV, and high-resolution images and Energy Dispersive X-ray Spectrometry (EDS) spectra were obtained using a Philips CM200 FEG STEM.

3. Results and discussion

In α-Al_2O_3, the sulfide nanocrystals exhibit strong faceting and tend to be elongated parallel to the surface (Fig. 1). Electron- and X-ray diffraction techniques were used to determine the crystal structure and orientation of the sulfide precipitates. When formed in alumina, the ZnS and CdS precipitates have the wurtzite structure with the major axes aligned $[0\,0\,1]_{Al_2O_3} \parallel [0\,0\,1]_{Zns}$. The PbS precipitates have the cubic rocksalt structure (e.g., as galena) and are aligned with two principle orientations: $[0\,0\,1]_{Al_2O_3} \parallel [0\,0\,1]_{PbS}$ and $[0\,0\,1]_{Al_2O_3} \parallel [1\,1\,1]_{PbS}$. In the case of the ZnS and PbS precipitates, individual nanocrystals appear to have coalesced into a single layer continuous for several

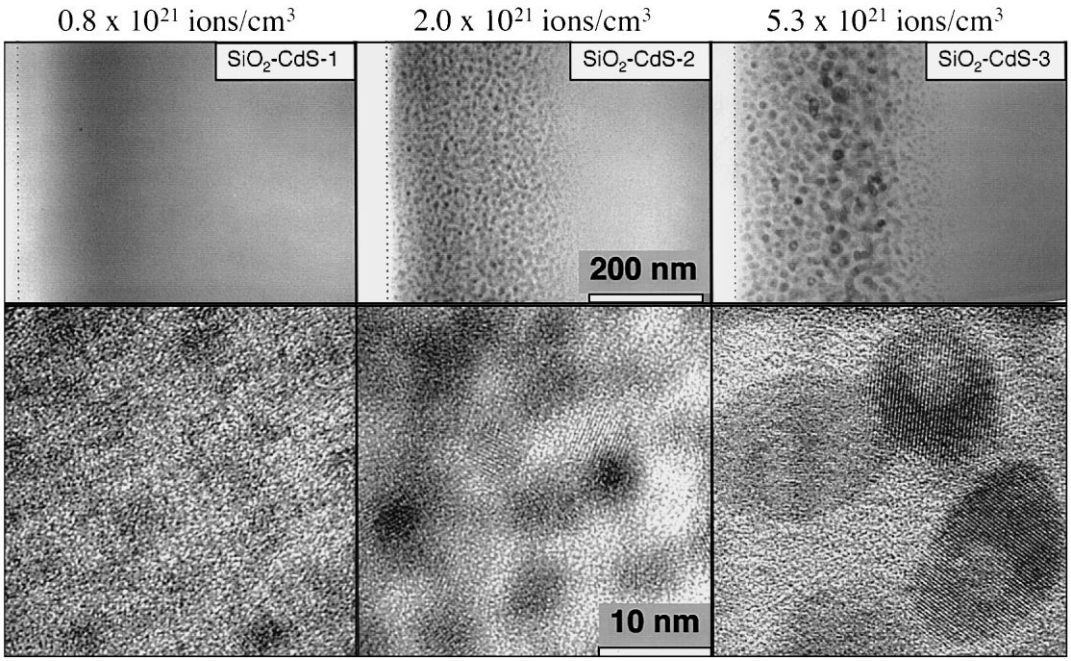

Fig. 4. Cross-sectional micrographs (top) and corresponding high-resolution TEM micrographs (bottom) for the three SiO_2–CdS multi-energy specimens. The surface is marked by the dotted line.

hundred nanometers (Fig. 1). This layer is "kinked" in those locations where some of the large nanocrystals that joined the layer were located at different depths. These results suggest that a single 2-dimensionally continuous sulfide layer could, in principle, be formed in alumina by implanting a higher ion dose.

The depth–concentration profiles for implanted Zn, Cd, or Pb obtained by RBS (Fig. 2), agree well with the observed depth-dependent distribution of precipitates (Fig. 1). The concentration profiles in Fig. 2 are "sharper" than those obtained prior to annealing, but the amount of implanted material (given by the area under the curves) remained nearly constant. The RBS profiles obtained for sulfur were similar to those in Fig. 2, but the scatter in the data was considerably larger due to its low atomic mass.

All three sulfides were also formed after implantation and annealing of a fused silica host, as determined by X-ray and electron diffraction. The ZnS and CdS precipitates formed in fused silica are randomly oriented and have the wurtzite structure, although in the case of ZnS, a minor zincblende component was also detected. The PbS nanocrystals have the cubic rocksalt structure. No additional phases were detected by X-ray diffraction. Concentration profiles for Pb, Cd, and Zn in SiO_2 after annealing were obtained from the RBS spectra (Fig. 2). Implanted Pb and Cd remain in the near-surface region, similar to the case for all three elements in α-Al_2O_3. The Zn profiles were unusual, however, in that the zinc concentration appeared to increase near the calculated end-of-range of the implanted ions, and a small amount of zinc appears to have diffused deeper into the specimen (Fig. 2).

The ZnS precipitates formed in fused silica have a strongly bimodal size distribution (Fig. 3). A band of large precipitates is located near the calculated end-of-range of the implanted ions. These large nanocrystals were observed in both the multi-energy and single-energy implants and occurred even in samples annealed for only 6 min (Fig. 3). This band of large precipitates was not present, however, prior to annealing the specimen.

In addition to the ZnS nanocrystals, precipitates with a spherulitic "snowflake" shape were observed to extend from the end-of-range into the deeper parts of the fused silica host except at the lowest ion doses (Fig. 3). Selected-area and convergent-beam electron diffraction and high-resolution imaging indicated that these structures are actually polycrystalline aggregates of γ-Zn_2SiO_4, a rarely reported phase known to occur upon the devitrification of SiO_2:ZnO glass compositions [5]. The formation of these various microstructural features was not noticeably affected when annealed in a neutral (Ar only) as compared to a reducing (Ar+4% H_2) environment.

The microstructure and size distributions in the case of the CdS nanocrystals produced in fused silica (Fig. 4) were different than for the case of ZnS. The size distribution was monomodal and the spread of precipitate sizes, as measured by the standard deviation, was lower (Table 1). Optical absorption spectra for these specimens are given in Ref. [6]. The results in Table 1 show that the mean size can be changed from ~9 to ~5 nm by reducing the concentration of implanted ions from 5×10^{21} to 8×10^{20} ions/cm^3. An interesting feature of the largest CdS precipitates is the presence of a central light-contrast structure. The contrast in the central area could not be reversed by tilting the specimen (i.e., it was always light). These initial observations suggest that this internal feature is, in fact, a void – a conclusion supported by initial Electron Energy Loss Spectrometry (EELS) results.

The size distribution of the PbS nanocrystals formed in fused silica was markedly different from the other sulfides (Fig. 5). At high ion doses, the nanocrystals showed a bimodal size distribution; however in this case, the largest nanocrystals were formed at the center of the implant profile. This finding is consistent with the RBS results which showed that the Pb-concentration profile sharpened during thermal annealing. The actual implanted concentration is higher for the SiO_2–PbS specimens at an equivalent ion dose because of the short range of the Pb ions at the implant energies used. The Bohr exciton radius for PbS is ~180 nm, so at a low ion dose (specimen SiO_2–PbS-1), virtually all of the nanoparticles should show quantum confinement effects.

For all three sulfides, reducing the ion dose has the effect of narrowing the size distribution (as measured by the standard deviation) and also results in smaller nanocrystals (Table 1, Fig. 3–5). A narrower range of sizes is obtained in the fused silica host than in crystalline α-Al_2O_3. Multiple energy overlaps can assist these parameters by providing a relatively constant concentration of the implanted species. For example, the multi-energy, low-dose ZnS implants into SiO_2 give a relatively narrow size distribution, and the formation of large nanocrystals at the end-of-range is almost entirely suppressed.

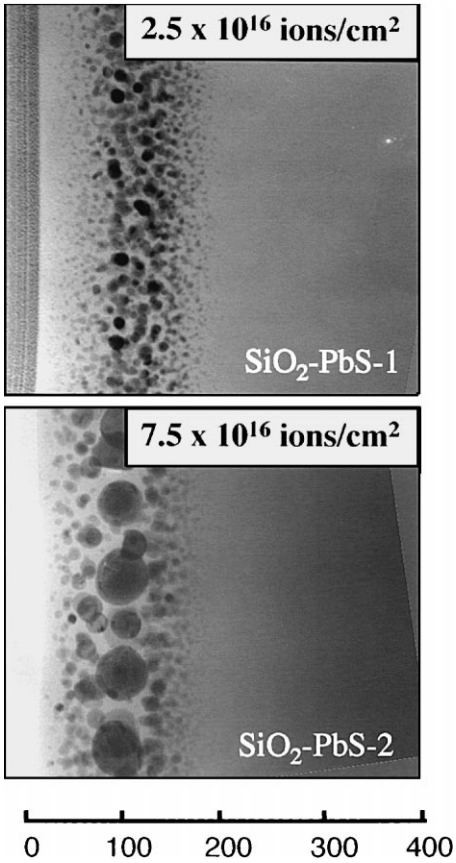

Fig. 5. Cross-sectional bright-field micrographs showing the distribution of PbS nanocrystals in fused silica. The depth scale is in nanometers.

4. Conclusions

The microstructure and size distributions of sulfide nanocrystal precipitates produced in fused silica and α-Al_2O_3 by ion-implantation techniques were investigated using cross-sectional TEM. Several unusual and unexpected features were observed, including strongly bimodal size distributions, the formation of a new phase (e.g., γ-Zn_2SiO_4) in the samples implanted with Zn+S, and central voids in the larger CdS nanocrystals. Work is ongoing to explain the origin of these features. All of these microstructures were suppressed in low-dose specimens, and the size distributions were considerably narrower. The size distribution is further reduced by using fused silica instead of a crystalline host material.

Acknowledgements

A.M. acknowledges support from the Natural Sciences and Engineering Research Council of Canada. Electron microscopy was performed at the SHaRE Facility at ORNL. Oak Ridge National Laboratory is managed by Lockheed Martin Energy Research Corp. for the US Department of Energy under contract number DE-AC05-96OR22464.

References

[1] J.D. Budai, C.W. White, S.P. Withrow, R.A. Zuhr, J.G. Zhu, Mat. Res. Soc. Symp. Proc. 452 (1997) 89.
[2] C.W. White, J.D. Budai, A. Meldrum, S.P. Withrow, R.A. Zuhr, E. Sonder, A. Puretzky, D.B. Geohegan, J.G. Zhu, D.O. Henderson, Mat. Res. Soc. Symp. Proc 504, in press.
[3] C. Bonafos, B. Garrido, M. Lopez, A. Romano-Rodriguez, O. Gonzáles-Varona, A. Pérez-Rodriguez, J.R. Morante, Appl. Phys. Lett. 72 (1998) 3488.
[4] J.P. McCaffrey, B.T. Sullivan, J.W. Fraser, D.L. Callahan, Micron 27 (1996) 407.
[5] J. Williamson, F.P. Glasser, Phys. Chem. Glasses 5 (1964) 52.
[6] C.W. White, A. Meldrum, J.D. Budai, S.P. Withrow, E. Sonder, R.A. Zuhr, D.M. Hembree, M. Wu, D.O. Henderson, these Proceedings (IBMM98), Nucl. Instr. and Meth. B 148 (1999).